Korean J. Chem. Eng., **31**(11), 1985-1993 (2014)
DOI: 10.1007/s11814-014-0140-1

pISSN: 0256-1115
eISSN: 1975-7220

Optimal Ru particle size for selective CO oxidation in H_2 over Ru/κ-Al_2O_3

Jung Eun Park and Eun Duck Park†

Department of Chemical Engineering and Department of Energy Systems Research, Ajou University, Wonchun-dong, Yeongtong-gu, Suwon 443-749, Korea
(*Received 6 April 2014 • accepted 13 May 2014*)

Abstract−Ru/κ-Al_2O_3 catalysts with different Ru dispersions were prepared by controlling the pretreatment conditions, and were applied to selective CO oxidation in H_2. The prepared catalysts were characterized by N_2 physisorption, transmission electron microscopy, temperature-programmed oxidation, CO chemisorption, and O_2 chemisorption. The Ru dispersion decreased with increasing reduction and oxidation temperature of Ru/κ-Al_2O_3. The turnover frequency for CO oxidation in H_2 increased as the Ru particle size increased from 2.2 to 3.6 nm, whereas the apparent activation energy decreased as the Ru particle size increased from 2.2 to 3.4 nm for 1% Ru/κ-Al_2O_3. However, larger Ru particles were not always favorable for the selective CO oxidation in H_2 because H_2 oxidation was also promoted by these catalysts. In the case of the 1 wt% Ru/κ-Al_2O_3 catalyst, Ru nanoparticles of approximately 3 nm appeared to be optimal for the selective CO oxidation in H_2 on the basis that they provided the widest temperature window, resulting in complete removal of CO even in the presence of H_2O and CO_2.

Keywords: Selective CO Oxidation, Ru Catalysts, κ-Al_2O_3, Size Effect, Hydrogen

INTRODUCTION

Hydrogen is considered a clean fuel because water is the only product of its combustion. Because H_2 does not exist in its pure form in nature, it must be synthesized from various resources. It is generally accepted that fossil fuels are still an economic hydrogen source to satisfy the current consumption of hydrogen, because the mass production of hydrogen from water by using solar energy is not currently economically feasible. The efficiency of hydrogen utilization can be improved by using fuel cells where the chemical energy is directly transformed into electricity. Polymer electrolyte membrane fuel cells (PEMFCs) offer several advantages, including high power density, easy start-up, and low operation temperature [1]. However, PEMFCs require high purity hydrogen as the fuel, which necessitates the use of a rather complex fuel processor, in which conventional hydrocarbons are transformed into hydrogen through a series of catalytic processes, including steam reformation and the water-gas shifter.

Because 0.5-1% CO exists in the generated hydrogen stream after the water-gas shifter, an additional step is required to clean up the residual CO in the hydrogen-rich stream. Preferential CO oxidation (PROX) has been proposed as one of most plausible candidates to achieve this goal [2]. In the PROX system, CO oxidation ($CO+(1/2)O_2 \rightarrow CO_2$), H_2 oxidation ($H_2+(1/2)O_2 \rightarrow H_2O$), CO methanation ($CO+3H_2 \rightarrow CH_4+H_2O$), CO_2 methanation ($CO_2+4H_2 \rightarrow CH_4+2H_2O$), and the water-gas shift reaction ($CO+H_2O \leftrightarrow CO_2+H_2$) may occur concurrently because all of the reactants (CO, CO_2, H_2, O_2, and H_2O) coexist in the system. Consequently, undesired reactions, such as H_2 oxidation, CO methanation, and CO_2 methanation, must be minimized during PROX.

A number of catalyst systems, including noble metal [3] and metal oxide catalysts [4-8], have been reported for the PROX. Noble metal catalysts have generally been reported to show higher PROX activity, especially at low temperatures, than metal oxide catalysts [9]. Among the unpromoted noble metal catalysts, the Ru-based catalyst exhibited the highest PROX activity [10,11]. The Ru-based catalyst exhibits the distinguishing feature of also being active in CO methanation, unlike other noble metal catalysts [12]. Recent research has pinpointed the effect of certain factors, such as the types of Ru precursors [13,14], pre-treatment conditions [13-16], and types of supports [14-20] on the PROX activity.

The particle size of Ru has been reported to be critical for complete CO oxidation [21,22] and PROX [19,23]. Joo et al. [21] prepared Ru nanoparticles within the size range 2-6 nm, and found that the catalytic activity for CO oxidation increased with size. We also observed the size effect of Ru on the PROX activity in reactions over Ru/SiO_2 and Ru/γ-Al_2O_3, where the PROX activity increased with Ru particle size [19, 23]. However, larger Ru particles are not always better for the PROX because H_2 oxidation as well as CO oxidation can proceed faster over them, resulting in a decrease in the CO_2 selectivity. For example, although Ru/α-Al_2O_3 with the lowest Ru dispersion showed the highest low-temperature PROX activity among Ru catalysts supported on various aluminum oxides with different crystalline phases, such as α-Al_2O_3, κ-Al_2O_3, γ-Al_2O_3, η-Al_2O_3, δ-Al_2O_3, and θ-Al_2O_3, this catalyst could not achieve full CO conversion [18]. Under the same reaction conditions, Ru/κ-Al_2O_3 resulted in full CO conversion at relatively low reaction temperatures [18]. Compared with other supports with high surface areas, κ-Al_2O_3 is also favorable for the PROX, where external mass transfer of oxygen is critical, because of its macroporous nature [24].

For practical applications, PROX catalysts should have a wide temperature window for complete CO removal. From this perspec-

†To whom correspondence should be addressed.
E-mail: edpark@ajou.ac.kr

tive, Ru/κ-Al_2O_3, a promising PROX catalyst, was selected for the evaluation of the effect of the Ru particle size on the PROX activity with the overarching aim to develop a more efficient PROX catalyst. Because κ-Al_2O_3 is prepared under more severe conditions than the pretreatment conditions adopted to adjust the Ru particle size, the original textural properties of κ-Al_2O_3 can be preserved during the pretreatment, and the effect of the Ru particle size on the PROX activity can be exclusively examined in this study.

EXPERIMENTAL PROCEDURE

1. Preparation of Catalysts

The Ru/κ-Al_2O_3 catalyst was prepared by an incipient wetness impregnation method, starting from an aqueous solution of ruthenium nitrosylnitrate ($Ru(NO)(NO_3)_3 \cdot xH_2O$, Aldrich) and κ-Al_2O_3, which was obtained after calcinations of gibbsite (Samchun Chem.) at 1,273 K for 4 h [18]. The Ru contents were fixed at 0.5 wt% and 1 wt%. The impregnated catalyst was dried overnight in an oven at 393 K, and reduced in a hydrogen stream for 1 h at different temperatures. The reduction temperature is included in the catalyst name to differentiate each catalyst: 1% Ru/κ-Al_2O_3-R773 indicates the 1 wt% Ru/κ-Al_2O_3 catalyst reduced at 773 K. Some of the 0.5 wt% Ru/κ-Al_2O_3 catalysts were pretreated by bringing 0.5% Ru/κ-Al_2O_3-R773 into contact with 10 mol% O_2 in He for 1 h at different temperatures (473, 500, and 573 K) to further increase the Ru particle size. These catalysts were also reduced a second time for 1 h at 773 K prior to reaction and characterization. The calcination temperature is also included in the catalyst name: 0.5% Ru/κ-Al_2O_3-C473 indicates the 0.5 wt% Ru/κ-Al_2O_3 catalyst reduced at 773 K, oxidized at 473 K with the gas stream of 10 mol% O_2 in He, and finally reduced at 773 K. For comparison, the commercial 0.5 wt% Ru/γ-Al_2O_3 catalyst was purchased from Aldrich and used after reduction in H_2 for 1 h at 573 K.

2. Characterization of Catalysts

N_2 physisorption was carried out on a Micromeritics ASAP 2020 system at 77 K. The specific surface area of κ-Al_2O_3 calculated using the Brunauer-Emmett-Teller (BET) method was determined to be 18.3 m^2/g, and its total pore volume and average pore diameter were calculated to be 0.20 mL/g and 38 nm, respectively. The pore size distribution was obtained from the desorption branch of the N_2 adsorption/desorption isotherm using the BJH formula. The N_2 adsorption/desorption and pore size distribution data are displayed in Fig. S1.

The Ru content was confirmed using inductively coupled plasma-optical emission spectrometry (ICP-OES, Varian 710-ES).

The average particle size of Ru was estimated using transmission electron microscopy (TEM) images obtained on a Tecnai G^2 F30 S-Twin (FEI) microscope operated at an acceleration voltage of 300 kV.

Pulse chemisorption measurements for CO and O_2 were performed using an Autochem 2910 unit (Micromeritics) equipped with a thermal conductivity detector (TCD) to measure the consumption of each gas. Prior to the measurement, the catalysts were reduced under 10% H_2/Ar flow at a flow rate of 30 mL/min for 1 h at 573 K, and then cooled to room temperature. Chemisorption was at 300 K in a He stream at a flow rate of 30 mL/min, using a pulse chemisorption technique in which 500 μL pulses of each gas were injected until a saturation level was reached. In the case of O_2 chemisorption, additional measurements were also made at 373 K.

Temperature-programmed oxidation (TPO) was conducted using the same Autochem 2910 unit as for chemisorption measurements. A water trap composed of silica gel was used to remove moisture from the effluent stream at 273 K before the TCD. Prior to the experiment, the catalyst was reduced in H_2 at 573 K for 1 h, and then cooled to room temperature under He flowing at a rate of 30 mL/min. The TPO was performed using 2% O_2/He at a flow rate of 30 mL/min, in the temperature range from 313 K to 573 K, at a heating rate of 10 K/min, while monitoring the TCD signals.

3. Catalytic Activity Test

The activity of the catalysts for PROX was evaluated using a small fixed-bed reactor in which a quartz reactor (internal diameter=3 mm and length=345 mm) was installed inside a split-type tube furnace. A K-type thermocouple was installed inside the reactor to measure the reaction temperature, which was controlled with a PID temperature controller (Ilhae System). For the screening tests, 0.10 g of catalyst without any diluent was brought into contact with the reactant gas, composed of 1 mol% CO, 1 mol% O_2, 50 mol% H_2, 20 mol% CO_2, and 10 mol% H_2O balanced with He, at a flow rate of 100 mL/min. The steady-state catalytic activity was measured at different reaction temperatures.

The kinetic data were obtained under differential reactor conditions by decreasing the amount of catalyst to achieve less than 15% CO conversion. An excessive amount of α-Al_2O_3 was homogeneously mixed with the catalyst to prevent formation of hot spots in the catalyst bed. The feed comprised 1 mol% CO, 1 mol% O_2, and 50 mol% H_2 balanced with He.

The reactants and products were separated with a packed column (Carbosphere), and analyzed online by gas chromatograph (HP 5890A) equipped with a TCD. The CO conversion, O_2 conversion, and CH_4 yield were calculated by using the following formulas:

$$\text{CO conversion } (\%) = \frac{[CO]_{in} - [CO]_{out}}{[CO]_{in}} \times 10 \quad (1)$$

$$O_2 \text{ conversion } (\%) = \frac{[O_2]_{in} - [O_2]_{out}}{[O_2]_{in}} \times 10 \quad (2)$$

$$CH_4 \text{ yield } (\%) = \frac{[CH_4]_{out}}{[CO]_{in}} \times 10 \quad (3)$$

where $[CO]_{in}$ and $[O_2]_{in}$ are the concentrations of CO and O_2 in the incoming stream and $[CO]_{out}$, $[O_2]_{out}$ and $[CH_4]_{out}$ are the concentrations of CO, O_2, and CH_4 in the outgoing stream, respectively. The detection limit of $[CO]_{out}$ was 10 ppm.

A moisture trap was installed before the gas chromatograph to remove moisture formed during the reaction.

RESULTS AND DISCUSSION

Because CO and O_2 are not only well-known probe molecules for characterization of metal catalysts but also main reactants for the PROX, the CO and O_2 chemisorption of the 1 wt% Ru/κ-Al_2O_3 catalysts was analyzed, and the results are in Table 1. Based on the amount of chemisorbed CO and the assumption that one CO molecule is linearly chemisorbed on one surface Ru atom, the fraction of surface Ru atoms relative to the total Ru atom content of the catalyst can be calculated; this parameter is termed the Ru dispersion. The

Table 1. Physicochemical properties of 1 wt% Ru/κ-Al_2O_3 catalysts reduced at different temperatures

Catalyst	[CO]/[Ru][a]	$[O_2]$/[Ru][b]	$[O_2]$/[Ru][c]	Ru particle size[d] (nm)	Temperature range for full CO conversion (K)[e]	E_a[f] [kJ/mol]
1% Ru/κ-Al_2O_3-R773	0.35	0.29	0.36	2.2±0.8	384-425	102
1% Ru/κ-Al_2O_3-R873	0.29	0.10	0.32	2.5±1.0	388-438	90
1% Ru/κ-Al_2O_3-R973	0.13	0.06	0.26	3.1±0.7	363-444	75
1% Ru/κ-Al_2O_3-R1073	0.11	n.d.	0.22	3.4±1.5	383-421	68
1% Ru/κ-Al_2O_3-R1173	0.06	n.d.	0.19	3.6±2.2	383-435	69

[a]CO chemisorption was carried out at 300 K
[b]O_2 chemisorption was carried out at 300 K
[c]O_2 chemisorption was carried out at 373 K
[d]Average Ru particle size was determined from TEM images
[e]Reaction conditions: feed composition: 1 mol% CO, 1 mol% O_2, 50 mol% H_2, 20 mol% CO_2, and 10 mol% H_2O balanced with He. space velocity=1,000 mL/min/g_{cat}
[f]Reaction conditions: 1 mol% CO, 1 mol% O_2, and 50 mol% H_2 balanced with He

Ru dispersion for the 1 wt% Ru/κ-Al_2O_3 catalysts that was reduced at different temperatures decreased in the following order: 1% Ru/κ-Al_2O_3-R773>1% Ru/κ-Al_2O_3-R873>1% Ru/κ-Al_2O_3-R973>1% Ru/κ-Al_2O_3-R1073>1% Ru/κ-Al_2O_3-R1173, which indicates that the Ru dispersion for the 1 wt% Ru/κ-Al_2O_3 catalyst decreased with increasing reduction temperature. Because the Ru dispersion is inversely proportional to the Ru particle size, it can be deduced that the Ru particle size increased with increasing reduction temperature. O_2 chemisorption measurements were also performed at 300 K for the 1 wt% Ru/κ-Al_2O_3 catalysts, and the results are in Table 1. The amount of chemisorbed O_2 for the 1 wt% Ru/κ-Al_2O_3 catalysts decreased in the following order: 1% Ru/κ-Al_2O_3-R773>1% Ru/κ-Al_2O_3-R873>1% Ru/κ-Al_2O_3-R973. In the cases of 1% Ru/κ-Al_2O_3-R1073 and 1% Ru/κ-Al_2O_3-R1173, no detectable chemisorbed O_2 was found. This indicates that the amount of O_2 chemisorbed at 300 K for the Ru/κ-Al_2O_3 catalyst also decreased with increasing Ru particle size. O_2 chemisorption measurements were also conducted at 373 K for the same catalysts. As presented in Table 1, the amount of chemisorbed O_2 decreased in the following order: 1% Ru/κ-Al_2O_3-R773>1% Ru/κ-Al_2O_3-R873>1% Ru/κ-Al_2O_3-R973>1% Ru/κ-Al_2O_3-R1073>1% Ru/κ-Al_2O_3-R1173. This also indicates that the amount of O_2 chemisorbed at 373 K for the Ru/κ-Al_2O_3 catalyst also decreased with increasing Ru particle size. Notably, the amount of O_2 chemisorbed at 373 K was higher than the amount of O_2 chemisorbed at 300 K for the same catalyst. The O_2 chemisorption data obtained at 300 and 373 K reveal that O_2 chemisorption proceeds at higher temperatures over larger Ru particles than over smaller counterparts.

The TPO experiment was carried out for the 1 wt% Ru/κ-Al_2O_3 catalyst that was reduced at different temperatures as shown in Fig. 1. The TPO peaks stem from the oxidation of chemisorbed H_2, O_2 chemisorption, and the bulk oxidation of metallic Ru into RuO_2 [14]. A broad TPO peak was observed for all 1 wt% Ru/κ-Al_2O_3 catalysts in the temperature range from 300 to 573 K. However, the intensity of the peak in the TPO pattern varied for each catalyst. The TPO peak area for the catalysts decreased in the following order: 1% Ru/κ-Al_2O_3-R773>1% Ru/κ-Al_2O_3-R873≈1% Ru/κ-Al_2O_3-R973>1% Ru/κ-Al_2O_3-R1073>1% Ru/κ-Al_2O_3-R1173. This indicates that the extent of Ru oxidation for the 1 wt% Ru/κ-Al_2O_3 catalyst decreased with increasing Ru particle size.

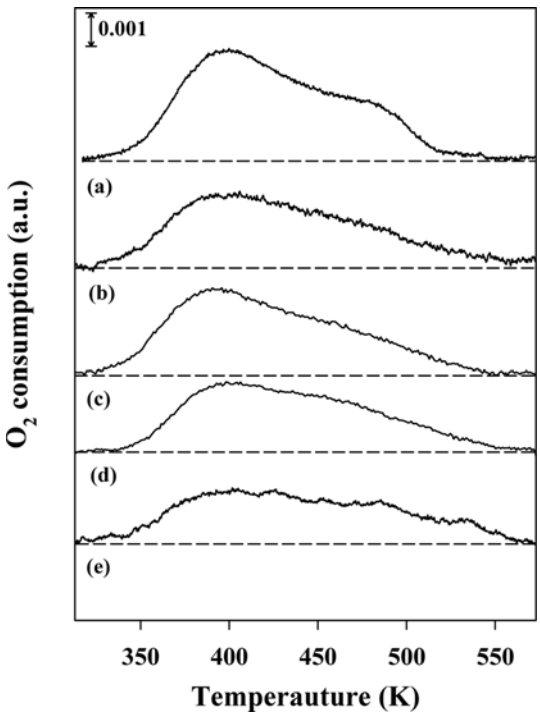

Fig. 1. Temperature-programmed oxidation (TPO) patterns of 1% Ru/κ-Al_2O_3 catalysts reduced at different temperatures such as 773 K (a), 873 K (b), 973 K (c), 1,073 K (d), and 1,173 K (e).

To derive more direct information on the particle size of Ru for the 1 wt% Ru/κ-Al_2O_3 catalysts reduced at different temperatures, TEM images of each catalyst were obtained (Fig. 2). The particle size distribution of the Ru particles for each catalyst was also obtained and is presented in the inset in Fig. 2. As listed in Table 1, the average Ru particle size determined from the particle size distribution for 1 wt% Ru/κ-Al_2O_3 increased with an increase in the reduction temperature, which is in agreement with the CO and O_2 chemisorption data.

To determine the effect of the surface concentration of Ru parti-

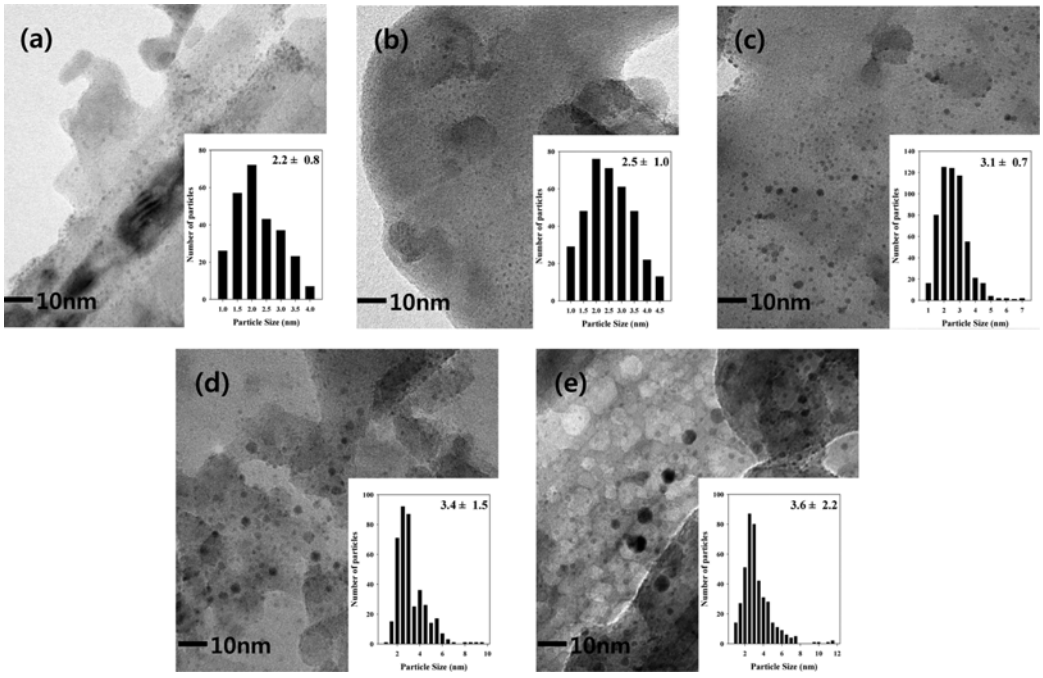

Fig. 2. Bright-field TEM images of 1 wt% Ru/κ-Al_2O_3 catalysts reduced at different temperatures: 1% Ru/κ-Al_2O_3-R773 (a), 1% Ru/κ-Al_2O_3-R873 (b), 1% Ru/κ-Al_2O_3-R973 (c), 1% Ru/κ-Al_2O_3-R1073 (d), and 1% Ru/κ-Al_2O_3-R1173 (e).

Table 2. Physicochemical properties of 0.5 wt% Ru/γ-Al_2O_3 and 0.5 wt% Ru/κ-Al_2O_3 catalysts pretreated under different conditions

Catalyst	[CO]/[Ru][a]	Ru particle size[b] (nm)	Temperature range for full CO conversion (K)[c]
0.5% Ru/γ-Al_2O_3-R573	0.37	2.5±0.5	-
0.5% Ru/κ-Al_2O_3-R773	0.55	<1.0	417-473
0.5% Ru/κ-Al_2O_3-R1173	0.40	2.1±4.6	409-479
0.5% Ru/κ-Al_2O_3-C473	0.23	2.7±8.1	403-480
0.5% Ru/κ-Al_2O_3-C500	0.18	2.9±10.4	404-433
0.5% Ru/κ-Al_2O_3-C573	0.08	n.d.	-

[a]CO chemisorption was carried out at 300 K
[b]Average Ru particle size was determined from TEM images
[c]Reaction conditions: feed composition: 1 mol% CO, 1 mol% O_2, 50 mol% H_2, 20 mol% CO_2, and 10 mol% H_2O balanced with He. space velocity =1,000 mL/min/g_{cat}.

cles on the Ru dispersion during the pretreatment, 0.5 wt% Ru/κ-Al_2O_3 catalysts were also prepared under different pretreatment conditions. CO chemisorption measurements were used to determine the Ru dispersion for each catalyst, as summarized in Table 2. The Ru dispersion of the 0.5 wt% Ru/κ-Al_2O_3 catalyst decreased with increasing reduction temperature, which is similar to the behavior observed for the 1 wt% Ru/κ-Al_2O_3 catalysts. However, the data in Tables 1 and 2 clearly show that the Ru dispersion of the 0.5 wt% Ru/κ-Al_2O_3 catalyst is much higher than that of the 1 wt% Ru/κ-Al_2O_3 catalysts for similar pretreatment conditions. This is quite reasonable because the probability of metal sintering should increase with increasing surface concentration of metal particles. Notably, the 0.5 wt% Ru/κ-Al_2O_3 catalyst reduced at a temperature as high as 1,173 K had a high Ru dispersion. Therefore, even more severe pretreatment conditions were adopted, in which the catalyst was oxidized with oxygen at elevated temperatures [23,25]. Table 2 clearly shows that the Ru dispersion decreased noticeably with increasing oxidation temperature. This implies that the oxidizing environment is more favorable for Ru sintering than the reducing atmosphere.

TEM images of the 0.5 wt% Ru/Al_2O_3 catalysts pretreated under different conditions were obtained to determine the particle size distribution of Ru metal (Fig. 3). The average Ru particle size in the commercial 0.5 wt% Ru/γ-Al_2O_3 catalyst was determined to be 2.5± 0.5 nm. For the 0.5 wt% Ru/κ-Al_2O_3 catalysts, the average Ru particle size increased with increasing reduction and oxidation temperature. Notably, much larger Ru particles could be formed under oxidizing environments at lower temperatures compared with the cases under reducing environments. Furthermore, a rather broad particle size distribution could be obtained for the 0.5 wt% Ru/κ-Al_2O_3 catalysts pretreated with O_2. In the case of the 0.5 wt% Ru/κ-Al_2O_3 catalyst pretreated with 10 mol% O_2 in He at 573 K, it was difficult to estimate the average Ru particle size owing to the presence of large agglomerates of Ru particles.

The evaluation of the PROX activity of the 1 wt% Ru/κ-Al_2O_3 catalysts reduced at different temperatures is summarized and their results are shown in Fig. 4. The PROX activity for the 1 wt% Ru/κ-Al_2O_3 catalysts, i.e., CO conversion at low temperatures, appeared to decrease in the following order: 1% Ru/κ-Al_2O_3-R973~1% Ru/κ-Al_2O_3-R873>1% Ru/κ-Al_2O_3-R1073>1% Ru/κ-Al_2O_3-R1173> 1% Ru/κ-Al_2O_3-R773. Full CO conversion was achieved with all of the catalysts in the temperature range from 388 to 421 K, even in the presence of CO_2 and H_2O. The widest temperature window was observed for the 1% Ru/κ-Al_2O_3-R973 catalyst, with a CO concentration of less than 10 ppm in the exiting stream, even in the presence of CO_2 and H_2O. Above 444 K, the CO conversion declined

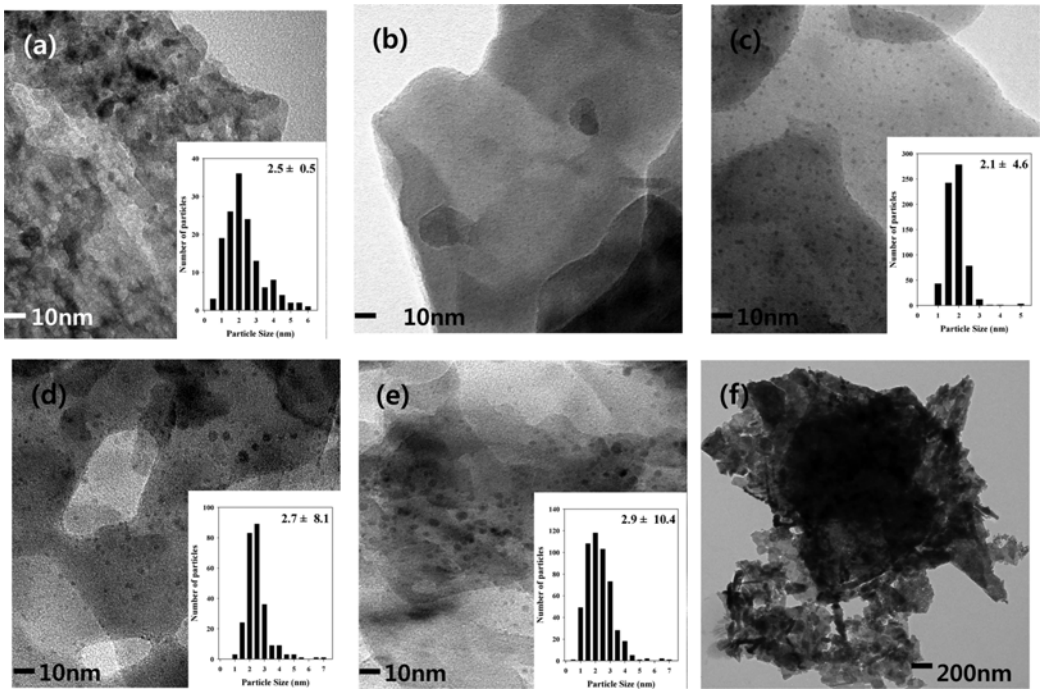

Fig. 3. Bright-field TEM images of various 0.5 wt% Ru/Al_2O_3 catalysts: 0.5% Ru/γ-Al_2O_3-R573 (a), 0.5% Ru/κ-Al_2O_3-R773 (b), 0.5% Ru/κ-Al_2O_3-R1173 (c), 0.5% Ru/κ-Al_2O_3-C473 (d), 0.5% Ru/κ-Al_2O_3-C500 (e), and 0.5% Ru/κ-Al_2O_3-C573 (f).

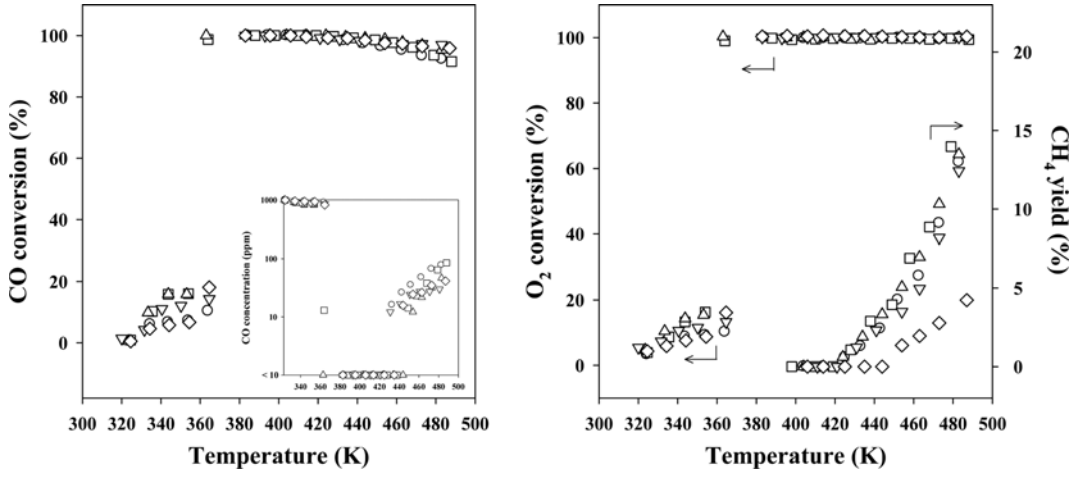

Fig. 4. CO conversion, exit CO concentration, O_2 conversion, and CH_4 yield for the selective CO oxidation with increasing reaction temperature over 1 wt% Ru/κ-Al_2O_3 catalysts reduced at different temperatures such as 773 K (○), 873 K (□), 973 K (△), 1,073 K (▽), and 1,173 K (◇). Space velocity=1,000 mL/min/g_{cat}. Feed composition: 1 mol% CO, 1 mol% O_2, 50 mol% H_2, 20 mol% CO_2, and 10 mol% H_2O balanced with He.

with increasing reaction temperature irrespective of the catalyst, ascribed to the predominance of H_2 oxidation over CO oxidation at high temperatures. In addition to oxidation of CO and H_2, methanation of CO and CO_2 occurs at high temperatures. CH_4 formation was observed in the presence of all the catalysts when the O_2 conversion was 100% (Fig. 4). The CH_4 yield for the Ru/κ-Al_2O_3 catalysts decreased in the following order: 1% Ru/κ-Al_2O_3-R773~1% Ru/κ-Al_2O_3-R873~1% Ru/κ-Al_2O_3-R973>1% Ru/κ-Al_2O_3-R1073 >>1% Ru/κ-Al_2O_3-R1173, which indicates that the CH_4 yield decreased with increasing Ru particle size of the Ru/κ-Al_2O_3 catalysts. Tada et al. [26] also reported a negative dependence on the Ru particle size for CO methanation over supported Ru catalysts.

The PROX activity was also measured for 0.5 wt% Ru/κ-Al_2O_3 catalysts reduced at 773 and 1,173 K and the commercial 0.5 wt% Ru/γ-Al_2O_3 catalyst was also evaluated under the same reaction conditions for comparison. As shown in Fig. 5, the CO conversion increased to about 90% as the reaction temperature increased to 409 K for the reaction over 0.5 wt% Ru/γ-Al_2O_3. This maximum CO conversion was maintained from 409 to 429 K, whereas the CO conversion decreased at temperatures above 429 K. In contrast, the CO conversion increased steadily with increasing reaction temperature for the reaction over the 0.5 wt% Ru/κ-Al_2O_3 catalyst reduced at

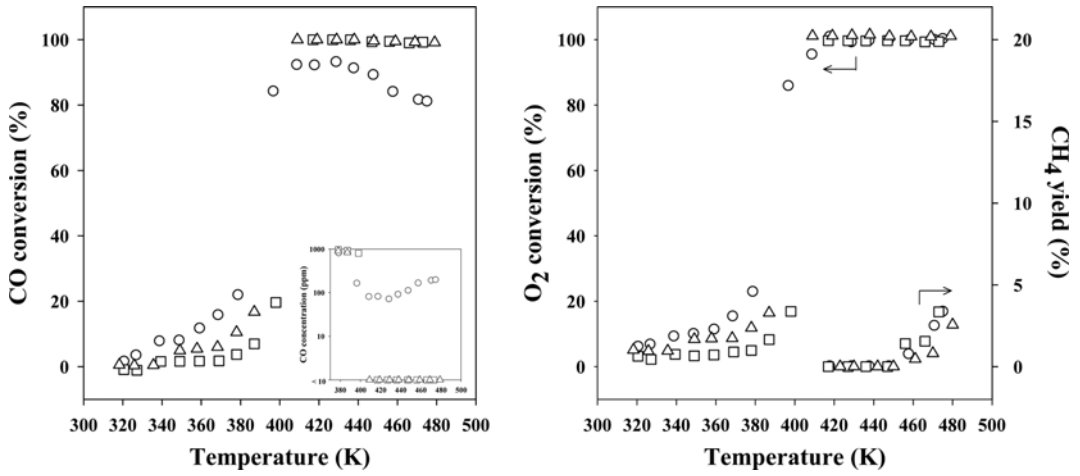

Fig. 5. CO conversion, exit CO concentration, O_2 conversion, and CH_4 yield for the selective CO oxidation over supported Ru catalysts: 0.5% Ru/γ-Al_2O_3-R573 (○), 0.5% Ru/κ-Al_2O_3-R773 (□), 0.5% Ru/κ-Al_2O_3-R1173 (△). Space velocity=1,000 mL/min/g_{cat}. Feed composition: 1 mol% CO, 1 mol% O_2, 50 mol% H_2, 20 mol% CO_2, and 10 mol% H_2O balanced with He.

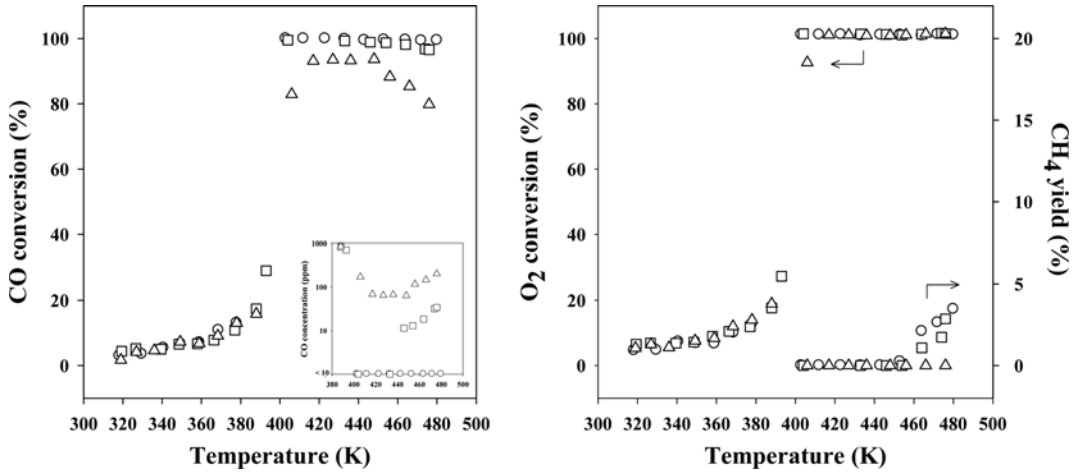

Fig. 6. CO conversion, exit CO concentration, O_2 conversion, and CH_4 yield for the selective CO oxidation over supported Ru catalysts: 0.5% Ru/κ-Al_2O_3-C473 (○), 0.5%Ru/κ-Al_2O_3-C500 (□), and 0.5%Ru/κ-Al_2O_3-C573 (△). Space velocity=1,000 mL/min/g_{cat}. Feed composition: 1 mol% CO, 1 mol% O_2, 50 mol% H_2, 20 mol% CO_2, and 10 mol% H_2O balanced with He.

773 K and reached 100% at 417 K. The exit CO concentration was less than 10 ppm over this catalyst in the temperature range from 417 to 473 K. Relative to the 0.5 wt% Ru/κ-Al_2O_3 catalyst reduced at 773 K, higher CO conversion at low temperatures and a wider temperature window were observed for the 0.5 wt% Ru/κ-Al_2O_3 catalyst reduced at 1,173 K with complete removal of CO. Considering the Ru dispersion and average Ru particle size for the 0.5 wt% Ru/γ-Al_2O_3 and 0.5 wt% Ru/κ-Al_2O_3 catalysts reduced at 773 and 1,173 K, the low-temperature PROX activity increased with increasing Ru particle size, irrespective of the support. In the case of the 0.5 wt% Ru/γ-Al_2O_3 catalyst, complete removal of CO was not accomplished even though this catalyst showed the highest CO conversion under the condition that the O_2 conversion was lower than 100%, as shown in Fig. 5. Thus, the Ru particle size as well as the support are important factors for controlling the PROX activity. CH_4 formation was observed only when the O_2 conversion was 100%.

To exclude the effect of the support while examining the effect of the Ru particle size on the PROX activity over a wider range, 0.5 wt% Ru/κ-Al_2O_3 catalysts were pretreated with a stream containing oxygen at different temperatures and applied to the PROX. As shown in Fig. 6, the CO conversion increased steadily with increasing reaction temperature over 0.5% Ru/κ-Al_2O_3-C473 and reached 100% conversion in the range from 403 to 480 K. This catalyst exhibits superior PROX activity relative to 0.5% Ru/κ-Al_2O_3-R1173 (see Fig. 5). Considering the Ru dispersion and average Ru particle size of these catalysts (Table 2), larger Ru particles appear to be favorable for low-temperature PROX activity. Similar CO conversions were obtained with the 0.5% Ru/κ-Al_2O_3-C500 and 0.5% Ru/κ-Al_2O_3-C473 catalysts if the O_2 conversion was lower than 100%, even though 0.5% Ru/κ-Al_2O_3-C500 has larger Ru particles than 0.5% Ru/κ-Al_2O_3-C473. However, 0.5% Ru/κ-Al_2O_3-C500 showed a narrower temperature window than 0.5% Ru/κ-Al_2O_3-C473, achieving complete removal of CO. This implies that the Ru particle size affects the low-temperature PROX activity and temperature window accomplishing complete CO removal. Furthermore, it can be concluded that there is an optimum Ru particle size for achieving

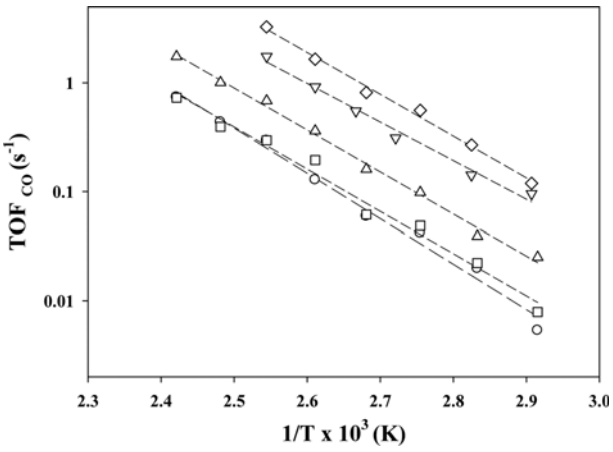

Fig. 7. Turnover frequency (TOF) for selective CO oxidation at different temperatures over 1% Ru/κ-Al_2O_3 catalysts reduced at different temperatures such as 773 K (○), 873 K (□), 973 K (△), 1,073 K (▽), and 1,173 K (◇). Feed composition: 1 mol% CO, 1 mol% O_2, and 50 mol% H_2 balanced with He.

high low-temperature PROX activity combined with a wide temperature window to achieve complete removal of CO. Similar CO conversion was achieved with 0.5% Ru/κ-Al_2O_3-C473 and 0.5% Ru/κ-Al_2O_3-C500 when the O_2 conversion was lower than 100%; however, 100% CO conversion was not achieved with 0.5% Ru/κ-Al_2O_3-C500 until 476 K. This strongly implies that H_2 oxidation is also promoted over large Ru particles resulting in a significant decrease in the CO_2 selectivity at high temperatures. CH_4 formation was observed only when the O_2 conversion was 100% and the CH_4 yield decreased with increasing Ru particle size.

The turnover frequency (TOF) for selective CO oxidation in H_2 was determined for the reaction over the 1 wt% Ru/κ-Al_2O_3 catalysts with various Ru dispersions at different reaction temperatures. As shown in Fig. 7, the TOF for the PROX decreased in the following order based on the catalysts: 1% Ru/κ-Al_2O_3-R1173>1% Ru/κ-Al_2O_3-R1073>1% Ru/κ-Al_2O_3-R973>1% Ru/κ-Al_2O_3-R873>1% Ru/κ-Al_2O_3-R773. The most active catalyst, 1% Ru/κ-Al_2O_3-R1173, exhibited negligible chemisorption of O_2 at 300 K during the O_2 chemisorption experiment, and exhibited the smallest uptake of O_2 up to 573 K during the TPO experiment. The apparent activation energy of the PROX over the Ru/κ-Al_2O_3 catalysts reduced at 773, 873, 973, 1,073, and 1,173 K was determined to be 102, 90, 75, 68, and 69 kJ/mol, respectively. The activation energy decreased with increasing Ru particle size. Behm and co-workers [16,25] reported that the activation energy for the PROX was 95±5 kJ/mol in the temperature range from 408 to 473 K over Ru/γ-Al_2O_3, where the average particle size of Ru was 3±1 nm.

The effect of the metal particle size on CO oxidation has been investigated by several groups. Atalik et al. [27] reported that the turnover frequency (TOF) for CO oxidation over Pt/γ-Al_2O_3 increased with decreasing Pt dispersion. The same result was obtained by Hershowitz et al. [28]. This might arise from the stronger adsorption of CO on smaller Pt particles. On the other hand, the TOFs for CO oxidation over supported gold catalysts increased with decreasing gold particle size in the range from 3 to 10 nm [29]. This can be explained in terms of the occurrence of the CO oxidation at the perimeter interfaces between the metallic gold, which functions as a CO adsorption site, and the support for O_2 adsorption [30]. In the case of Ru-based catalysts, the activity of the Ru nanoparticles for CO oxidation was reportedly improved by increasing the size of the Ru particles within the range 2-6 nm [21]. We also reported that larger Ru particles are favorable for the PROX compared with smaller particles in the case of Ru/SiO_2 and Ru/γ-Al_2O_3 [19,23]. The results of this study clearly support the claim that the PROX activity over Ru/κ-Al_2O_3 increases with increasing Ru particle size within the range from 2.2 to 3.6 nm.

It remains controversial whether the active phase of the Ru catalyst for CO oxidation is a nonoxidic phase [31] or the RuO_2 phase [32]. In any case, it is accepted that the most active structure of the Ru particle is the shell-core structure (RuO_2@Ru) in which the metallic Ru core is coated by an ultrathin RuO_2 film of 1-2 nm [32]. The activation energy for the CO oxidation reaction over this type of core-shell particle was reported to be approximately 80 kJ/mol [33]. On the other hand, the apparent activation energy for fully oxidized particles that are less active in the CO oxidation was determined to be approximately 100 kJ/mol [34]. It is worth mentioning that the apparent activation energy for the PROX over Ru/κ-Al_2O_3 decreased with increasing Ru particle size in the range from 2.2 to 3.4 nm in this work. Qadir et al. [22] compared two Ru-based catalyst systems with different Ru particle sizes of 2.8 and 6 nm for CO oxidation, and found that the larger 6 nm Ru nanoparticles were oxidized to a lesser extent than the smaller Ru 2.8 nm nanoparticles within the temperature range 50-200 °C under the given reaction conditions. They explained the higher catalytic activity of the larger nanoparticles in terms of the smaller extent of Ru oxidation: it was claimed that the smaller Ru nanoparticles form bulk RuO_2 on their surfaces, resulting in the lower catalytic activity. This strongly supports the claim that the core-shell type RuO_2 becomes stable as the size of the nanoparticle increases. Based on these considerations, the higher TOF for the PROX over the larger Ru particles can be explained in terms of the more stable core-shell structure of Ru. However, H_2 oxidation may also be promoted over the larger Ru particles, resulting in a decrease in the CO_2 selectivity. As shown in Tables 1 and 2, the Ru catalysts with the largest Ru particles did not guarantee the widest reaction temperature for achieving full CO conversion. Therefore, it can be concluded that there is an optimum Ru particle size for optimal PROX performance. For 1 wt% Ru/κ-Al_2O_3, the catalyst reduced at 973 K, which had a Ru dispersion of 13% and a Ru particle size of 3.1±0.7 nm, exhibited the widest temperature window, leading to full CO conversion. In the case of 0.5 wt% Ru/κ-Al_2O_3, the catalyst calcined at 473 K, which had a Ru dispersion of 23% and Ru particle size of 2.7±8.1 nm, showed the best PROX performance.

The Ru-based catalyst has been reported to suffer from deactivation during CO oxidation, especially under oxidizing conditions [35]. This is also related to the observation that the catalytic activity for CO oxidation is enhanced in the presence of H_2 [19,23]. Aβmann et al. [35] observed that the active oxide overlayer in RuO_2@Ru gradually became inactive as the RuO_2 layer became thicker than 1 to 2 nm under oxidizing conditions. Qadir et al. [36] also reported that bulk Ru oxide was easily formed on Ru catalysts, and that continuous deactivation of the Ru film was correlated with the irre-

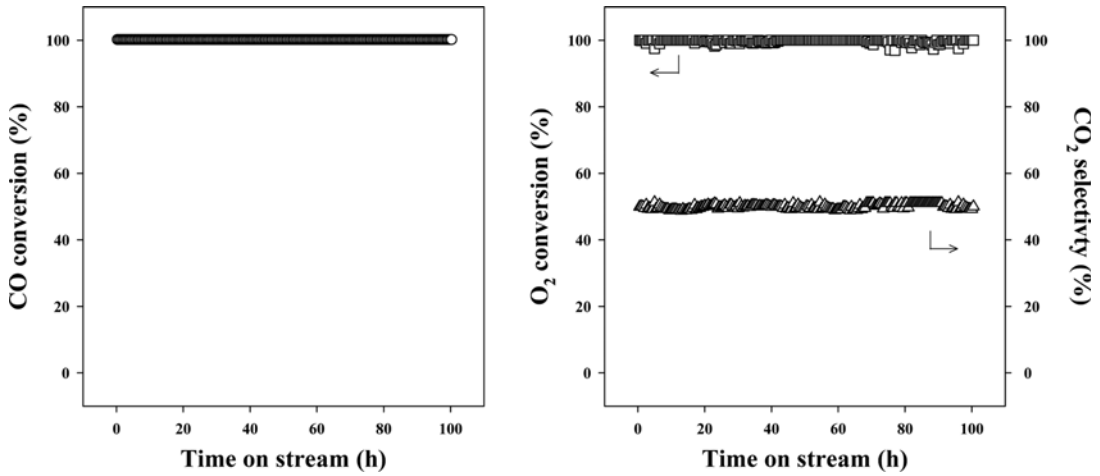

Fig. 8. CO conversion (○), O_2 conversion (□), and CO_2 selectivity (△) at 373 K as a function of reaction time over 1% Ru/κ-Al_2O_3-R973 catalyst. Space velocity=1,000 mL/min/g_{cat}. Feed composition: 1 mol% CO, 1 mol% O_2, 50 mol% H_2, 20 mol% CO_2, and 10 mol% H_2O balanced with He.

versible formation of bulk Ru oxide. Because the surface structure of the Ru catalyst can be altered to produce changes in the catalytic activity, the long-term stability of 1% Ru/κ-Al_2O_3-R973 for the PROX was evaluated. As shown in Fig. 8, full CO conversion was maintained at 373 K for 100 h, even in the presence of CO_2 and H_2O. Strongly reductive conditions might stabilize the active phase of the Ru catalyst.

CONCLUSIONS

Increasing the reduction temperature of 1 wt% Ru/κ-Al_2O_3 from 773 to 1,173 K increased the Ru particle size from 2.2 to 3.6 nm. The apparent activation energy for CO oxidation in the presence of H_2 decreased with increasing Ru particle size. Although the turnover frequency for CO oxidation in the presence of H_2 increased with increasing Ru particle size, the optimal size of Ru particles for 1 wt% Ru/κ-Al_2O_3 was around 3 nm for achieving complete CO removal over the widest temperature range in the presence of CO_2 and H_2O. Metal sintering during the reductive pretreatment was depressed with decreasing surface Ru concentration. In the case of the 0.5 wt% Ru/κ-Al_2O_3 catalyst, the highest low-temperature PROX activity and the widest temperature window were achieved with the Ru catalyst with an average Ru particle size of 2.7±8.1 nm, resulting in complete CO removal.

ACKNOWLEDGEMENTS

This work was supported by the Next Generation Military Battery Research Center program of the Defense Acquisition Program Administration and Agency for Defense Development. This research was also supported by the Basic Science Research Program through the National Research Foundation of Korea (NRF), funded by the Ministry of Education (NRF-2009-0094046).

REFERENCES

1. C. Song, *Catal. Today*, **77**, 17 (2002).
2. E. D. Park, D. Lee and H. C. Lee, *Catal. Today*, **139**, 280 (2009).
3. K. Liu, A. Wang and T. Zhang, *ACS Catal.*, **2**, 1165 (2012).
4. G. Avgouropoulos, T. Ioannides and H. Matralis, *Appl. Catal. B: Environ.*, **56**, 87 (2005).
5. B. Qiao, A. Wang, J. Lin, L. Li, D. Su and T. Zhang, *Appl. Catal. B: Environ.*, **105**, 103 (2011).
6. Z. K. Zhao, R. H. Jin, T. Bao, X. L. Lin and G. R. Wang, *Appl. Catal. B: Environ.*, **110**, 154 (2011).
7. Q. Zhang, X. Liu, W. Fan and Y. Wang, *Appl. Catal. B: Environ.*, **102**, 207 (2011).
8. J. E. Park and E. D. Park, *Catal. Lett.*, **144**, 607 (2014).
9. E.-Y. Ko, E. D. Park, K. W. Seo, H. C. Lee, D. Lee and S. Kim, *Catal. Today*, **116**, 377 (2006).
10. S. H. Oh and R. M. Sinkevitch, *J. Catal.*, **142**, 254 (1993).
11. Y. H. Kim, E. D. Park, H. C. Lee, D. Lee and K. H. Lee, *Catal. Today*, **146**, 253 (2009).
12. G. Xu and Z.-G. Zhang, *J. Power Sources*, **157**, 64 (2006).
13. A. Worner, C. Friedrich and R. Tamme, *Appl. Catal. A: Gen.*, **245**, 1 (2003).
14. S. Y. Chin, O. S. Alexeev and M. D. Amiridis, *Appl. Catal. A: Gen.*, **286**, 157 (2005).
15. M. Echigo and T. Tabata, *Appl. Catal. A: Gen.*, **251**, 157 (2003).
16. Y.-F. Han, M. Kinne and R. J. Behm, *Appl. Catal. B: Environ.*, **52**, 123 (2004).
17. Y. H. Kim, E. D. Park, H. C. Lee and D. Lee, *Appl. Catal. A: Gen.*, **366**, 363 (2009).
18. Y. H. Kim and E. D. Park, *Appl. Catal. B: Environ.*, **96**, 41 (2010).
19. Y. H. Kim, S.-D. Yim and E. D. Park, *Catal. Today*, **185**, 143 (2012).
20. I. Rosso, M. Antonini, C. Galletti, G. Saracco and V. Specchia, *Top. Catal.*, **30-31**, 475 (2004).
21. S. H. Joo, J. Y. Park, J. R. Renzas, D. R. Butcher, W. Huang and G. A. Somorjai, *Nano Lett.*, **10**, 2709 (2010).
22. K. Qadir, S. H. Joo, B. S. Mun, D. R. Butcher, J. R. Renzas, F. Aksoy, Z. Liu, G. A. Somorjai and J. Y. Park, *Nano Lett.*, **12**, 5761 (2012).
23. Y. H. Kim, J. E. Park, H. C. Lee, S. H. Choi and E. D. Park, *Appl. Catal. B: Environ.*, **127**, 129 (2012).
24. M. Kipnis and E. Volnina, *Appl. Catal. B: Environ.*, **98**, 193 (2010).

25. Y.-F. Han, M. J. Kahlich, M. Kinne and R. J. Behm, *Phys. Chem. Chem. Phys.*, **4**, 389 (2004).
26. S. Tada, R. Kikuchi, K. Urasaki and S. Satokawa, *Appl. Catal. A: Gen.*, **404**, 149 (2011).
27. B. Atalik and D. Uner, *J. Catal.*, **241**, 268 (2006).
28. M. Hershowitz, R. Holliday, M. B. Cutlip and C. N. Kenney, *J. Catal.*, **74**, 408 (1982).
29. M. Haruta, S. Tsubota, T. Kobayashi, H. Kageyama, M. J. Genet and B. Delmon, *J. Catal.*, **144**, 175 (1993).
30. M. Haruta, *J. New Mater. Electrochem. Syst.*, **7**, 163 (2004).
31. F. Gao and D. W. Goodman, *Phys. Chem. Chem. Phys.*, **14**, 6688 (2012).
32. H. Over, *Chem. Rev.*, **112**, 3356 (2012).
33. V. Narkhede, J. Aβmann and M. Muhler, *Z. Phys. Chem.*, **219**, 979 (2005).
34. J. T. Kiss and R. D. Gonzalez, *J. Phys. Chem.*, **88**, 892 (1984).
35. J. Aβmann, D. Crihan, M. Knapp, E. Lundgren, E. Loffler, M. Muhler, V. Narkhede, H. Over, M. Schmid, A. P. Seitsonen and P. Varga, *Angew. Chem. Int. Ed.*, **44**, 917 (2005).
36. K. Qadir, S. M. Kim, H. Seo, B. S. Mun, F. A. Akgul, Z. Liu and J. Y. Park, *J. Phys. Chem.*, *C* **117**, 13108 (2013).